



# A molecular brush with thermoresponsive poly(2-ethyl-2-oxazoline) side chains: a structural investigation

Jia-Jhen Kang<sup>1</sup> · Kaltrina Shehu<sup>1,2</sup> · Clemens Sachse<sup>3</sup> · Florian A. Jung<sup>1</sup> · Chia-Hsin Ko<sup>1</sup> · Lester C. Barnsley<sup>4,5</sup> · Rainer Jordan<sup>3</sup> · Christine M. Papadakis<sup>1</sup>

Received: 8 April 2020 / Revised: 19 June 2020 / Accepted: 6 July 2020 / Published online: 5 August 2020  
© The Author(s) 2020

## Abstract

The thermoresponsive behavior of a poly(2-oxazoline)-based molecular brush is investigated in aqueous solution. The molecular brush under study, PiPOx<sub>100</sub>-g-PEtOx<sub>17</sub>, has a poly(2-isopropenyl-2-oxazoline) (PiPOx) backbone grafted with thermoresponsive poly(2-ethyl-2-oxazoline) (PEtOx) side chains. Since the backbone degree of polymerization is only a factor of ~6 higher than the ones of the side chains, it features an architecture between a star-like polymer and a comb-like polymer. Its aqueous solution exhibits lower critical solution temperature (LCST) behavior with a cloud point temperature  $T_{cp} = 40.5$  °C at 30 g L<sup>-1</sup>. The temperature-dependent structural evolution is disclosed using dynamic light scattering (DLS) and small-angle neutron scattering (SANS). An increase of the molecular brush size is found upon heating from room temperature to  $T_{cp}$ , which is attributed to the extension of the backbone resulting from the dehydration and collapse of the side chains. Above  $T_{cp}$ , the size decreases again, which indicates the collapse of the whole molecular brush. Large aggregates are found to be present in the solution in the temperature range 25–50 °C. These become more compact, as the temperature is increased across  $T_{cp}$ .

**Keywords** Molecular brushes · Thermoresponsive polymers · Dynamic light scattering · Small-angle neutron scattering

## Introduction

Molecular brushes are densely grafted polymers having a rather rigid conformation due to the steric hindrance between the

polymeric side chains on the backbone [1, 2]. Their molecular structure can be adjusted by modifying the architectural parameters, e.g., the grafting density and the molar masses of the backbone/side chains. Due to their versatility in structure along with the possibility to introduce a high number of functional segments, they are attractive candidates for various potential applications, such as carrier systems and photonic crystals [3–7].

The ratio between the backbone and the side chain lengths determines whether the molecular brush is of spherical-like or rod-like shape [8–11]. When the side chains are much longer than the backbone, the molecular brush has an architecture close to the one of a star-like polymer and therefore assumes a spherical shape. On the other hand, when the backbone is significantly longer than the side chains, its architecture is close to a bottlebrush.

It is of interest to study the effect of the conformational changes of stimuli-responsive side chains on the overall brush conformation. For instance, side chains from polymers that exhibit lower critical solution temperature (LCST) behavior in aqueous solution are expected to show strong effects. LCST-type polymers are water-soluble at low temperatures and become more and more hydrophobic, as the temperature

**Electronic supplementary material** The online version of this article (<https://doi.org/10.1007/s00396-020-04704-6>) contains supplementary material, which is available to authorized users.

✉ Christine M. Papadakis  
papadakis@tum.de

- <sup>1</sup> Fachgebiet Physik der weichen Materie, Physik-Department, Technische Universität München, James-Frank-Straße 1, 85748 Garching, Germany
- <sup>2</sup> Present address: Heinz-Maier-Leibnitz-Zentrum (MLZ), Technische Universität München, Lichtenbergstr. 1, 85748 Garching, Germany
- <sup>3</sup> Professur für Makromolekulare Chemie, Fakultät Chemie und Lebensmittelchemie, Technische Universität Dresden, Mommsenstraße 4, 01069 Dresden, Germany
- <sup>4</sup> Jülich Centre for Neutron Science (JCNS) at Heinz Maier-Leibnitz Zentrum, Forschungszentrum Jülich GmbH, Lichtenbergstraße 1, 85748 Garching, Germany
- <sup>5</sup> Australian Synchrotron, ANSTO, 800 Blackburn Road, Clayton 3168, Australia

is increased. At the cloud point temperature  $T_{cp}$ , the polymers dehydrate, and the chains collapse, which is referred to as the coil-to-globule transition [12, 13]. Except for extremely dilute solutions, the collapse of the polymer chains is followed by the formation of aggregates, leading to an increased opacity of the solutions.

Aqueous solutions of molecular brushes, whose backbones are grafted with LCST-type polymers, also feature LCST behavior. The resulting structural evolution of the molecular brush upon heating depends largely on its architecture [14]. Li et al. investigated the thermoresponsive behavior of a molecular brush with a short backbone and long side chains (degrees of polymerization of the backbone and the side chains of  $N_{bb} = 33$  and  $N_{sc} = 73$ ), where the side chains are the LCST-type poly(*N*-isopropylacrylamide) (PNIPAM) [15]. Using small-angle neutron scattering (SANS) in a temperature range from 10 °C to around  $T_{cp}$  of PNIPAM (~32 °C), a gradual decrease of the size upon heating was found up to 30 °C, which was attributed to the collapse of the side chains. Above  $T_{cp}$ , large aggregates form in the solution. Another study considers molecular brushes which have a backbone that is significantly longer than the PNIPAM side chains ( $N_{bb} = 558$ ,  $N_{sc} = 13$ ) [16]. Dynamic light scattering (DLS) reveals a slight decrease of the hydrodynamic radius from 20 to 31 °C, followed by a sharp drop at 32 °C. Under atomic force microscopy, a cylinder-to-globule transition of the brush conformation was observed. This overall collapse was attributed to the enhanced intra-molecular interactions between the side chains upon heating; therefore, as the side chains collapse and attract each other, the backbone coils up, resulting in the globular shape of molecular brush at 32 °C.

Poly(2-alkyl-2-oxazoline)s with short alkyl substituents are another class of thermoresponsive LCST-type polymers, which have attracted attention in biomedical applications because of their biocompatibility and their tunable thermoresponsivity [17–19]. When the substituent is an ethyl group, the polymer, poly(2-ethyl-2-oxazoline) (PEtOx), has a cloud point of  $T_{cp} \cong 61$ –70 °C, depending on the molar mass and the solution concentration [20, 21]. Furthermore, short PEtOx chains (with degrees of polymerization below 100) do not exhibit LCST behavior in the range 0 to 100 °C [22, 23]. Nevertheless, several studies showed that star-like or comb-like polymers with short PEtOx arms ( $N_{sc} < 100$ ) display LCST behavior [10, 24–26]. Structural studies were carried out around the cloud points of these molecular brushes with PEtOx side chains using SANS and/or DLS [10, 26]. Different dependences of the molecular size on temperature were found: with the grafting density (fraction of backbone monomers which are attached with a side chain) varying from 70 to 100%, the different  $N_{bb}$  to  $N_{sc}$  ratios were considered to be the main reason for the size dependence on the temperature around  $T_{cp}$ . Besides, coexisting individually

dissolved brushes and large aggregates were detected from room temperature to  $T_{cp}$  in the system.

In the present study, a molecular brush having a poly(2-isopropenyl-2-oxazoline) backbone and PEtOx side chains is investigated in aqueous solution. Its backbone and side chain lengths are  $N_{bb} = 100$  and  $N_{sc} = 17$ ; thus, their ratio lies between the ones described above. At room temperature, the molecular brush is soluble in water. The focus is on the conformational changes of the brushes around  $T_{cp}$  and the presence of aggregates. The manuscript is structured as follows: firstly, the cloud point  $T_{cp}$  of the solution is identified by turbidimetry; subsequently, the temperature-dependence of the hydrodynamic radius is investigated by DLS, and finally, the inner structures of the molecular brushes and their aggregates are resolved by SANS.

## Materials and methods

### Materials

The molecular brush under study,  $PiPOx_{100}$ -g- $PEtOx_{17}$ -NBocPip, is poly(2-oxazoline)-based, featuring a poly(2-isopropenyl-2-oxazoline) ( $PiPOx$ ) backbone and poly(2-ethyl-2-oxazoline) (PEtOx) side chains, which are end-capped with *tert*-butyloxycarbonyl groups (NBocPip) in order to facilitate the polymer characterization. The chemical structure is shown in Fig. 1a. For simplicity, it is called  $PiPOx_{100}$ -g- $PEtOx_{17}$  in the following.  $PiPOx_{100}$ -g- $PEtOx_{17}$  has a high grafting density, i.e., there is a side chain attached on almost every monomer of the polymeric backbone. The number-average molar mass,  $M_n$ , is 132 kg mol<sup>-1</sup> and the dispersity,  $D$ , is 1.13, as determined by size exclusion chromatography (SEC); see below. The synthesis of  $PiPOx_{100}$ -g- $PEtOx_{17}$  was performed according to a modified method to a previous report [27]. The fully extended length of the  $PiPOx$  backbone and the PEtOx side chains of the molecular brushes are estimated by summing up the monomer length considering the C-C bond length (0.154 nm), the C-N bond length (0.147 nm), and the bond angle (109.5°) [28], to be 25 nm and 6 nm, respectively. Thus, the largest possible length in the longitudinal direction of the brush is the one of the fully stretched backbone plus two times that of the side chains, namely, 37 nm.

### $PiPOx_{100}$

To 150 mL tetrahydrofuran, 3 mL  $iPOx$  (3.18 g, 28.6 mmol, 3% v/v) were added, and the temperature was equilibrated at -20 °C. Polymerization was initiated by addition of 0.1 mL *n*-butyl lithium in hexane (0.25 mmol, 2.5 M). After 30 min, the reaction was terminated with argon-saturated methanol (1.00 ml). Then, the solvent volume was reduced, diluted with

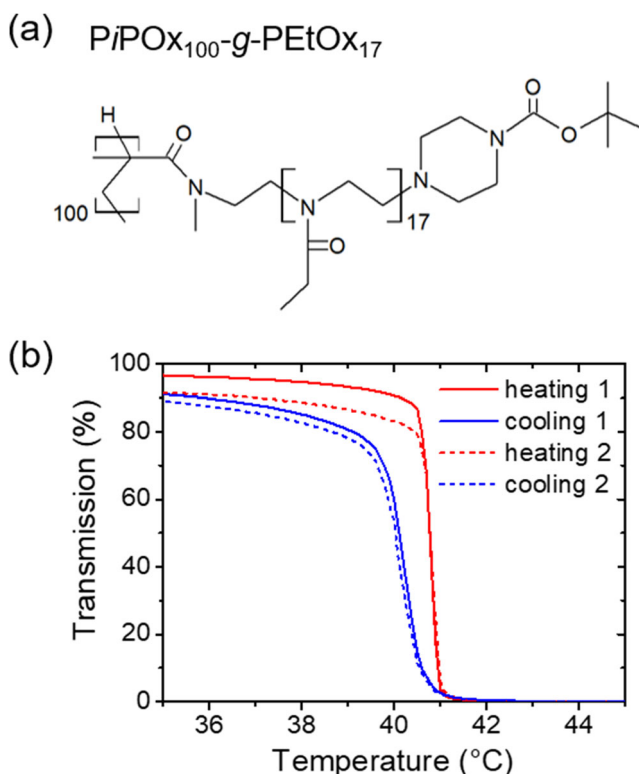


**Fig. 1** (a) Chemical structure of the molecular brush under study,  $PiPOx_{100}$ - $g$ - $PEtOx_{17}$ . (b) Light transmission versus temperature of a  $30\text{ g L}^{-1}$  solution of  $PiPOx_{100}$ - $g$ - $PEtOx_{17}$  in  $H_2O$ , measured during two heating and cooling runs, as indicated

chloroform, precipitated from diethyl ether three times, and lyophilized from water to obtain white polymer (2.8 g, 88%).  $^1H$  NMR (400 MHz,  $CDCl_3$ )  $\delta$  4.26–4.02 (m, 2H), 3.89–3.64 (m, 2H), 2.0–1.62 (m, 2H), 1.57–0.91 (m, 3H). FTIR:  $2942\text{ cm}^{-1}$  ( $\nu_{as}$  C-H, m),  $1652\text{ cm}^{-1}$  ( $\nu$  C=N, vs),  $1120\text{ cm}^{-1}$  ( $\nu_{as}$  C-O, s),  $983$ – $896\text{ cm}^{-1}$  (oxazoline ring skeleton vibration, s). SEC (RI):  $M_n = 11.1\text{ kg mol}^{-1}$ ,  $\bar{D} = 1.14$ .

#### $PiPOxOTf_{100}$

To a stirring solution of 215 mg  $PiPOx$  (1.93 mmol, 1 eq.) in 5.8 ml acetonitrile, 314 mg methyl triflate (2.08 mmol, 1.1 eq.) were added at room temperature and stirred for 16 h. The solvent was evaporated; the resulting yellowish solid was dissolved in dry acetonitrile and precipitated twice from dry diethyl ether. After evaporation of remaining solvent, the initiator salt was obtained as yellowish solid (520 mg, 94%) and processed as soon as possible. Reaction and purification were performed under dry and inert conditions using the *Schlenk*-technique.  $^1H$ -NMR (400 MHz,  $CD_3CN$ )  $\delta$  5.38–4.88 (m, 2H), 4.70–4.29 (m, 2H), 3.86–3.55 (m, 3H), 2.83–2.26 (m, 3H), 1.70–1.19 (m, 3H).

#### $PiPOx_{100}$ - $g$ - $PEtOx_{17}$ -NBocPip

An amount of 502 mg of  $PiPOxOTf$  (1.90 mmol) was dissolved in 28 mL acetonitrile and the 2.87 mg  $EtOx$  (29.01 mmol, 15 eq.) was added. The mixture was stirred at  $80\text{ }^\circ\text{C}$  overnight and cooled to room temperature. After termination with 2.5 mL *N*-Boc-piperazine (250 mg/mL in chloroform, 3.4 mmol, 1.8 eq.) for 24 h at room temperature, an excess of potassium carbonate was added for neutralization. After centrifugation, the polymer was dissolved in methanol/chloroform (3:1) and precipitated in diethyl ether three times. After lyophilization, the polymer was obtained as white solid (2.381 g, 69%).  $^1H$  NMR (400 MHz, MeOD)  $\delta$  4.04–3.37 (m, 676H), 2.69–2.22 (m, 38H), 1.47 (s, 9H), 1.22–1.00 (m, 51H). SEC (RI):  $\bar{D} = 1.18$ ,  $M_n = 58.7\text{ kg mol}^{-1}$ . SEC (MALLS):  $\bar{D} = 1.14$ ,  $M_n = 132\text{ kg mol}^{-1}$ . The refractive index increment  $dn/dc = 0.076\text{ mol g}^{-1}$ .

#### Size exclusion chromatography

SEC measurements were done on a system from Jasco (Groß-Umstadt, Germany) with a PU 2080 HPLC-pump, a JetStream II Plus column oven, equipped with one Gram 3000  $8 \times 300$  mm and one Gram 30  $8 \times 300$  mm column and dimethylacetamide (DMAc) with  $5\text{ g L}^{-1}$  LiBr and 1 vol%  $H_2O$  as the mobile phase at  $70\text{ }^\circ\text{C}$ . The system was calibrated with PMMA standards (PSS, Mainz, Germany). A Dawn DSP laser photometer at  $\lambda = 632.8\text{ nm}$  (Wyatt Technology, Dernbach, Germany) and an RI-930 RI detector (Jasco) were used for detection. Samples were dissolved in the mobile phase and filtered through  $0.2\text{ }\mu\text{m}$  PTFE syringe filters prior to the measurement. Refractive index increments  $dn/dc$  were determined using a differential refractometer DR1/b from SLS Systemtechnik (Denzlingen, Germany) in the concentration range of  $1$ – $5\text{ g L}^{-1}$  at a temperature of  $35\text{ }^\circ\text{C}$ .

#### Turbidimetry

Turbidity measurements were performed on a  $PiPOx_{100}$ - $g$ - $PEtOx_{17}$  solution at  $30\text{ g L}^{-1}$  in  $H_2O$ , using a Lambda 35 UV/VIS spectrometer equipped with a PTP-1 Peltier System (all from PerkinElmer, Germany) and controlled using the Templab software provided by the instrument supplier.  $T_{cp}$  of the molecular brush solution was determined by spectrophotometric detection of the changes in transmission of the polymer solution at  $\lambda = 500\text{ nm}$ , and the transmission values were normalized to that of the sample solution at  $25\text{ }^\circ\text{C}$ . The heating/cooling rate was  $1.0\text{ }^\circ\text{C min}^{-1}$ . The given value of  $T_{cp}$  was determined as the temperature corresponding to a 10% decrease in the optical transmission, and the uncertainty for  $T_{cp}$  is the temperature difference between two data points,  $0.1\text{ }^\circ\text{C}$ .

## Dynamic light scattering

DLS measurements were conducted on a  $\text{PiPO}_{\text{x}100}\text{-g-PEtOx}_{17}$  solution at  $30 \text{ g L}^{-1}$  in  $\text{D}_2\text{O}$ . The  $\text{D}_2\text{O}$  solvent was filtered before use to prepare the polymer solution. A LS Spectrometer from LS Instruments (Fribourg, Switzerland) was used, which was equipped with a goniometer and two avalanche photodiode detectors in pseudo cross correlation. The light source was a polarized HeNe laser (Thorlabs, Dachau, Germany) with a maximum power 21 mW and a wavelength  $\lambda = 632.8 \text{ nm}$ . The solution was filled in a cylindrical glass cuvette, having an outer diameter 5 mm and wall thickness 0.4 mm. The cuvette was mounted in a decalin bath, connected to a Julabo CF31 *Cryo-Compact Circulator* (JULABO, Seelbach, Germany) for temperature control. Data were collected during a temperature scan from 25 to 41 °C, i.e., up to  $T_{\text{cp}}$  of the solution, at a scattering angle  $2\theta = 90^\circ$ . At each temperature, the thermal equilibrium time was set to 10 min, and 20 measurements of a duration of 30 s were carried out. The scan procedure was repeated two times, and after the first time, the sample was left to equilibrate at 25 °C for 2.5 h. The normalized autocorrelation functions  $g_2(q, \tau)$  ( $q = 4\pi n \times \sin(\theta)/\lambda$  is the momentum transfer, with  $n$  being the refractive index of the solvent, and  $\tau$  is the delay time) were analyzed using the REPES algorithm implemented in the Gendist software [29, 30]. It yields the distribution of hydrodynamic radii  $A(R_h)$ , which is given in equal-area representation  $R_h A(R_h)$  vs.  $\log(R_h)$ . The  $R_h$  values were determined as the center of mass of each peak. At this, we neglect possible small deviations from pure translational diffusive behavior which might be present for anisotropic particles. The average value of  $R_h$  as well as the standard deviation were determined from the 20 measurements at each temperature.

## Small-angle neutron scattering

SANS experiments were conducted on a  $\text{PiPO}_{\text{x}100}\text{-g-PEtOx}_{17}$  solution at  $30 \text{ g L}^{-1}$  in  $\text{D}_2\text{O}$ . Measurements were performed at the KWS-1 instrument of the Jülich Centre for Neutron Science (JCNS) at the Heinz Maier-Leibnitz Zentrum (MLZ), Garching, Germany [31, 32]. With the neutron wavelength  $\lambda = 5 \text{ \AA}$  ( $\Delta\lambda/\lambda = 10\%$ ) and sample-to-detector distances (SDD) of 1.5 m, 8.0 m, and 20 m, a  $q$ -range of  $0.02\text{--}4.5 \text{ nm}^{-1}$  was covered ( $q = 4\pi \times \sin(\theta)/\lambda$ , where  $2\theta$  is the scattering angle). The exposure times at the 3 SDDs were 8 min, 15 min, and 30 min, respectively. The sample holder was a quartz glass cuvette (Hellma Analytics) with 2-mm neutron path length, and the cuvette was mounted in a thermostat (Peltier) to control the temperature. Data were collected from 25 to 50 °C, and the thermal equilibrium time at each temperature was 3 min.

The scattered intensity was recorded by a scintillation detector with an active area of  $60 \text{ cm} \times 60 \text{ cm}$  and a spatial resolution of  $5.3 \text{ mm} \times 5.3 \text{ mm}$ , and the intensity was brought to absolute value by plexiglass (poly(methyl methacrylate)). The intensity was corrected for the background from the solvent-filled cuvette, taking the transmissions into account. Such obtained intensity was azimuthally averaged to give plots of scattering intensity versus momentum transfer  $q$ , and the contribution from the  $\text{D}_2\text{O}$  solvent was subtracted. All operations were carried out using the software QtiKWS provided by JCNS.

## Model fitting of SANS data

The SANS data were modeled using the following expression:

$$I(q) = I_{\text{agg}}(q) + I_0 P_{\text{mb}}(q) S_{\text{HS}}(q) + I_{\text{fluct}}(q) + I_{\text{bkg}} \quad (1)$$

The scattering from large aggregates,  $I_{\text{agg}}(q)$ , was modeled by a modified Porod term, which is given by [33]:

$$I_{\text{Porod}}(q) = \frac{I_P}{q^\alpha} \quad (2)$$

$I_P$  is the scaling factor of the modified Porod term. When the aggregates are mass fractals, the Porod exponent  $\alpha$  ranges from  $5/3$  to 3, where  $\alpha = 5/3$  indicates loosely connected aggregates and  $\alpha = 3$  compact ones. When  $3 < \alpha < 4$ , the aggregates are compact and  $\alpha$  contains information on their surface structure:  $\alpha = 3$  is obtained for rough surfaces and  $\alpha = 4$  for smooth surfaces [34].

The second term,  $I_0 P_{\text{mb}}(q) S_{\text{HS}}(q)$ , is the scattering contribution from the individual molecular brushes.  $I_0$  is a scaling factor. As the form factor  $P_{\text{mb}}(q)$ , we chose the cylinder form factor,  $P_{\text{cyl}}(q)$ , which features the cross-sectional radius  $R$  as well as the length  $L$  of the cylindrical brushes [35–37].  $R$  and  $L$  are distributed according to Gaussian distributions, and their polydispersities are treated as free parameters. The polydispersity is defined as  $\sigma/X_{\text{avg}}$ , where  $\sigma$  is the standard deviation and  $X_{\text{avg}}$  is the central position of the Gaussian distribution. The form factor reads:

$$P_{\text{cyl}}(q) = \int_0^{\pi/2} \left[ \frac{J_1(qR\sin(a))}{qR\sin(a)} \frac{\sin(\frac{1}{2}qL\cos(a))}{\frac{1}{2}qL\cos(a)} \right]^2 \sin(a) da \quad (3)$$

where  $J_1$  is the first-order Bessel function, and  $a$  is the angle between the longitudinal axis of the cylinder and the scattering vector. The Percus-Yevick hard-sphere structure factor,  $S_{\text{HS}}(q)$ , was used to describe the spatial correlation between the brushes [38]:

$$S_{\text{HS}}(q) = \frac{1}{1 + 24\eta G(2R_{\text{HS}}q)/(2R_{\text{HS}})} \quad (4)$$

with

$$G(x) = \gamma \frac{\sin(x) - x \cos(x)}{x^2} + \delta \frac{2x \sin(x) + (2-x^2) \cos(x) - 2}{x^3} + \varepsilon \frac{-x^4 \cos(x) + 4(3x^2 - 6 \cos(x) + (x^3 - 6x) \sin(x) + 6)}{x^5} \quad (5)$$

where the functions  $\gamma$ ,  $\delta$ , and  $\varepsilon$  are defined as:

$$\gamma = \frac{(1 + 2\eta)^2}{(1-\eta)^4}; \delta = \frac{-6\eta(1 + \frac{\eta}{2})^2}{(1-\eta)^4}; \varepsilon = \frac{\gamma\eta}{2} \quad (6)$$

The average distance between the correlated molecular brushes is twice the hard-sphere radius,  $R_{HS}$ . The volume fraction occupied by the correlated brushes is the hard-sphere volume fraction,  $\eta$ .

The Ornstein-Zernike structure factor was used to model the concentration fluctuations within the molecular brush at small length scales,  $I_{\text{fluct}}(q)$  [39]. It reads:

$$I_{\text{fluct}}(q) = \frac{I_{oz}}{1 + (q\xi)^2} \quad (7)$$

$I_{oz}$  is the scaling factor and  $\xi$  the correlation length of the concentration fluctuations.

$I_{\text{bkg}}$  is the incoherent background and was treated as a free parameter due to precipitation of the brushes at high temperatures. The scattering length densities (SLD) of the PiPOx backbone, the PEtOx side chains, and the NBocPip end groups are calculated from the correspondingly mass densities to be  $1.23 \times 10^{-6} \text{ \AA}^{-2}$  [40],  $0.88 \times 10^{-6} \text{ \AA}^{-2}$  [41], and  $0.74 \times 10^{-6} \text{ \AA}^{-2}$  [42], respectively. The software SasView 4.2.2 was used for model fitting [43], taking the smearing effects into account.

## Results and discussion

To investigate the influence of the thermoresponsive behavior of the PEtOx side chains on the phase behavior and the structure of the PiPOx<sub>100</sub>-g-PEtOx<sub>17</sub> molecular brushes (Fig. 1a), turbidimetry, dynamic light scattering (DLS), and small-angle neutron scattering (SANS) measurements were carried out on aqueous solutions of the brushes in dependence on temperature. The polymer concentration was chosen at  $30 \text{ g L}^{-1}$ , either in H<sub>2</sub>O (for turbidimetry) or in D<sub>2</sub>O (for DLS and SANS). While turbidimetry indicates the cloud point,  $T_{\text{cp}}$ , DLS gives the temperature-dependent hydrodynamic radius of the molecular brushes and their aggregates. SANS reveals the shape, size, and inner structure of the brushes as well as their correlation.

The molecular brush under study consists of a water-soluble PiPOx backbone [44] and PEtOx side chains, which are LCST-type polymers. Figure 1b shows the light transmission data from temperature-resolved turbidimetry measurements of a  $30 \text{ g L}^{-1}$  PiPOx<sub>100</sub>-g-PEtOx<sub>17</sub> solution in H<sub>2</sub>O. During heating, the transmittance decreases slightly and shows a sharp drop at  $41 \text{ }^\circ\text{C}$ , which is also recovered during the second heating run. The cloud point is determined to be  $T_{\text{cp}} = 40.5 \pm 0.1 \text{ }^\circ\text{C}$  as the temperature where the transmission is 90%. Upon cooling, a hysteresis of ca.  $1 \text{ }^\circ\text{C}$  is observed, which is also reproducible.

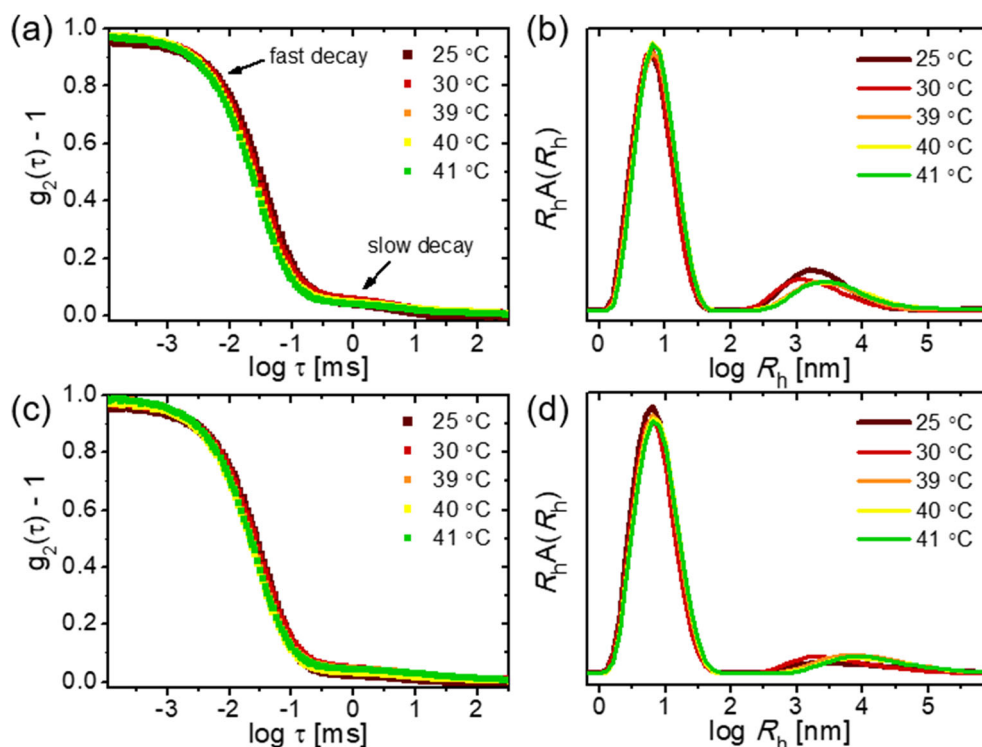
Based on previous results [20, 21], the short PEtOx side chains ( $N_{\text{sc}} = 17$ ) are expected to have a very high cloud point ( $T_{\text{cp}} > 100 \text{ }^\circ\text{C}$ ). The  $T_{\text{cp}}$  of the solution of densely grafted brushes is much lower, which may be due to the close proximity of the side chains [45]. In addition, the fact that the side chains are end-capped with the hydrophobic *tert*-butyloxycarbonyl group [46, 47] may also be responsible for the lowered  $T_{\text{cp}}$  [15].

DLS measurements were carried out from  $25$  to  $41 \text{ }^\circ\text{C}$ , i.e., in the one-phase state, where the solution is optically clear. The heating procedure was repeated twice with an equilibration time of  $2.5 \text{ h}$  at  $25 \text{ }^\circ\text{C}$  before the second scan. In this temperature range, the normalized intensity autocorrelation curves feature two decays (Fig. 2a, c), suggesting two kinds of diffusing particles in different sizes present in the solution. The fast mode has a rather high amplitude and is tentatively assigned to the diffusion of individual molecular brushes. The slow mode is rather weak and is presumably due to the diffusion of large aggregates. The corresponding distributions of hydrodynamic radii  $R_h$  (Fig. 2b, d) feature two peaks, with the fast one being narrower than the slow one. From the areas under the fast and slow peaks, it is seen that  $80$ – $90\%$  of the scattering intensity stem from the fast mode. This implies that the individually dissolved brushes constitute the majority in the solution, and only few aggregates are present. The hydrodynamic radius of the aggregates is found to range from several micrometers up to several tens of micrometers. This length scale is outside the detection range of DLS; thus, the hydrodynamic radius of the aggregates cannot be determined reliably.

The  $R_h$  values of the individually dissolved molecular brushes are shown in dependence on temperature in Fig. 3, where the results from the two scans are provided. Both scans show a slight increase of  $R_h$  from room temperature to  $T_{\text{cp}}$ , which might indicate a changing brush shape upon heating. As the molecular brushes are supposed to have a rod-like shape, the increase of  $R_h$  is most possibly due to an increase of size along the axial direction of the rod.

Comparing  $R_h$  in the two scans, it increases from  $7.8 \pm 0.4 \text{ nm}$  ( $25 \text{ }^\circ\text{C}$ ) to  $8.6 \pm 0.4 \text{ nm}$  ( $41 \text{ }^\circ\text{C}$ ) in the first scan, and from  $8.4 \pm 1.1 \text{ nm}$  ( $25 \text{ }^\circ\text{C}$ ) to  $9.3 \pm 1.0 \text{ nm}$  ( $41 \text{ }^\circ\text{C}$ ) in the second scan (Fig. 3). Thus, the thermoresponsive behavior

**Fig. 2** Representative DLS data at selected temperatures from the two heating scans of the 30 g L<sup>-1</sup> PiPO<sub>x100</sub>-g-PEtO<sub>x17</sub> solution in D<sub>2</sub>O. (a) and (c) The normalized autocorrelation curves from the first and the second scan, respectively. (b) and (d) The corresponding distribution functions of hydrodynamic radii,  $R_h$ , respectively. The temperatures are indicated in the graphs



of the individual molecular brushes is reproducible within the uncertainties. The minor inconsistency by  $\sim 0.5$  nm and the higher uncertainties in the second scan might also imply that the solution would need longer than 2.5 h of equilibration at 25 °C to reverse back to the stable equilibrium state at this temperature after having been heated above its cloud point.

To gain information about the structural evolution of the molecular brushes and their aggregates, SANS data were collected in a wide  $q$  range and in the temperature range between 25 and 50 °C, i.e., during heating through  $T_{cp}$ . Figure 4 shows the scattering data in dependence on temperature. They have several features in common: at the lowest  $q$  values ( $0.02$ – $0.06$  nm<sup>-1</sup>), the scattering intensity shows a decay, indicating

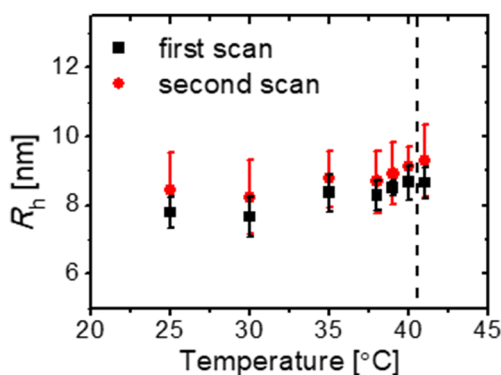


**Fig. 3** Hydrodynamic radius of the individually dissolved molecular brushes in dependence on temperature from the first (black squares) and the second (red circles) heating scan. The vertical dashed lines indicate  $T_{cp}$  of the solution, determined by turbidimetry

the presence of aggregates in the solution. Comparing data below and above  $T_{cp}$  (Fig. 4a and b), the  $q$ -dependence is steeper above  $T_{cp}$ . The scattering in the mid- $q$  region ( $0.06$ – $1$  nm<sup>-1</sup>) is due to the individually dissolved brushes, and the broad maximum at  $q \approx 0.2$  nm<sup>-1</sup> indicates that they are weakly correlated. Upon heating throughout the entire temperature range, the curves show only weak changes in the mid- $q$  region; only the position of the maximum moves to lower  $q$  values up to  $T_{cp}$  and to higher  $q$  values above, which is an indication of a varying distance between the brushes in the solution. In the high  $q$  region ( $1$ – $5$  nm<sup>-1</sup>), a shallow decay is present, which is assumed to be due to concentration fluctuations within the molecular brushes. This decay remains unchanged with temperature. Above  $T_{cp}$ , a steady decrease of the overall scattering intensity is noticeable (Fig. 4b), which is due to precipitation. At the end of the SANS measurement (50 °C), the precipitates are clearly visible in the cuvette. The amount of precipitation is estimated from the loss of the incoherent background. Based on our fitting results, the incoherent background drops from  $0.0139$  cm<sup>-1</sup> at 40 °C to  $0.0078$  cm<sup>-1</sup> at 50 °C. Thus, approximately 44% of the polymers in the solution precipitate between 40 and 50 °C. After storage at room temperature for a few weeks, the precipitates had re-dissolved, indicating the reversibility of the transition.

Model fitting of the SANS data enables to extract detailed structural information on the molecular brushes as well as on their aggregates. The Porod law is used to describe the scattering from the aggregates at low  $q$ , giving information on their compactness and surface roughness. As for modeling

the molecular brushes, judging from the backbone-to-side chain length ratio and the results from previous studies [10, 11, 48], the shape of the brushes is most likely to be ellipsoidal or cylindrical. After unsuccessful initial fits of the form factor of ellipsoids, the form factor of cylinders having a polydisperse radius and length gave good fits. The flexible cylinder model was tried as well; however, it gave large Kuhn lengths, pointing to a high stiffness of the cylinders, and the model was discarded again. Using the above described model for straight and polydisperse cylinders, the dimensions of the cylinders, i.e., the cross-sectional radius  $R$  and the length  $L$ , are determined. The cylinder form factor is combined with the Percus-Yevick hard-sphere structure factor, and the average distance between the brushes is deduced from the hard-sphere radius  $R_{HS}$ , along with the volume fraction occupied by the correlated brushes,  $\eta$ . The scattering due to the concentration fluctuations within the molecular brushes is described by the Ornstein-Zernike structure factor. Figure 4c shows the contributions to the model (Eq. 1) and the overall fit of the SANS data at 25 °C. Fits of the SANS data at the other temperatures

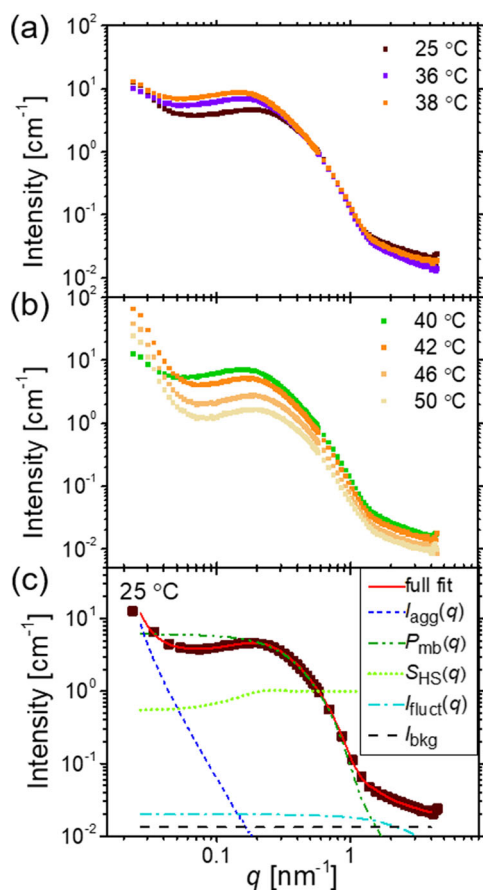


**Fig. 4** Representative SANS data of the 30 g L<sup>-1</sup> solution of PiPOx<sub>100</sub>-g-PEtOx<sub>17</sub> in D<sub>2</sub>O (a) from 25 to 38 °C and (b) from 40 to 50 °C. (c) Demonstration of a representative model fit to the SANS data at 25 °C using Eq. 1. For clarity, only every third data point is shown. The different contributions in Eq. 1 are indicated by different colors and line types

as well as the full parameter sets are given in the [Electronic Supplementary Material](#).

The molecular brushes are modeled by the cylinder form factor, and it is found that the cylinder length increases considerably with temperature, as  $T_{cp}$  is approached: between 25 and 38 °C, it grows from ~13 to ~21 nm, which amounts to an increase of 60% of its original value (Fig. 5a). In contrast, the cylinder radius stays constant at ~3 nm in this temperature range (Fig. 5a). The cylinders thus grow in length when heating from 25 to 38 °C, which is in line with the DLS results described above. Upon further heating, the cylinder length decreases from ~21 nm at 38 °C to ~12 nm at 50 °C, while the radius stays unchanged at ~3 nm. Thus, from room temperature to  $T_{cp}$ , the brushes extend, whereas further above  $T_{cp}$ , the brushes contract. It seems that they undergo a two-stage conformational change. The reason for the increase of the length of the molecular brushes may be that the PEtOx side chains dehydrate and shrink, resulting in a higher density near the backbone [49], which leads to a straightening of the backbone of the brushes. The following decrease might indicate

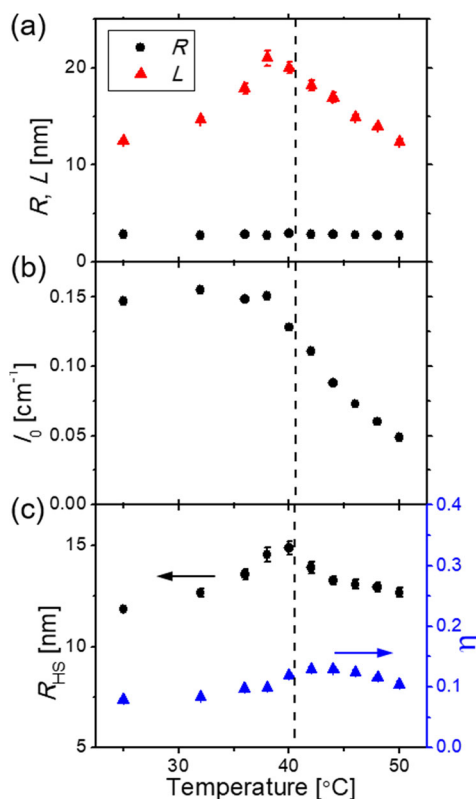


**Fig. 5** Parameters from model fitting to the SANS data of the 30 g L<sup>-1</sup> solution of PiPOx<sub>100</sub>-g-PEtOx<sub>17</sub> in D<sub>2</sub>O in dependence on temperature. (a) Dimensions from the cylinder form factor: radius  $R$  (black circles) and length  $L$  (red triangles). (b) Scaling factor of the cylinder form factor  $I_0$ . (c) Parameters from the hard-sphere structure factor: hard-sphere radius  $R_{HS}$  (black circles, left scale) and volume fraction  $\eta$  (blue triangles, right scale). The vertical dashed line indicates  $T_{cp}$  of the solution

the further dehydration of the side chains, resulting in the collapse of the entire molecular brush. It is worth mentioning that this conformational change is not reflected in a change of the cross-sectional radius  $R$ , which is probably due to the spatial restrictions in the lateral direction of the brush. A constant cross-sectional radius was also reported in other studies [50]. As for the scaling factor  $I_0$  of the cylinder form factor (Fig. 5b), it is unchanged from room temperature to 38 °C, and shows a steady decrease above 38 °C, which is tentatively attributed to the decrease in the number of dissolved molecular brushes in the solution. It could be that, above 38 °C, these brushes become a part of the aggregates, resulting in a decrease of  $I_0$ .

A rough idea about the PEtOx side chain length may be gained from the cylinder radius, namely,  $\sim 3$  nm at all temperatures. The PiPOx backbone length can be estimated by the cylinder length minus two times that of the side chains, which gives  $\sim 15$  nm at 38 °C, i.e. at its most stretched conformation. Comparing the cylinder length and the radius from model fitting (Fig. 5a) with the values calculated for the fully stretched backbone and side chains (see the Materials and methods section), we conclude that neither the backbone nor the side chains are fully stretched. This holds true even at 38 °C, where the brushes are most extended. This finding is consistent with previous findings [48].

The hard-sphere radius  $R_{HS}$  has a value of  $\sim 12$  nm at 25 °C and gradually increases to  $\sim 15$  nm upon heating up to 40 °C (Fig. 5c). From 40 to 50 °C,  $R_{HS}$  decreases to  $\sim 13$  nm. This dependence on temperature corresponds to the one of the

cylinder length very well; however, the average distance,  $2R_{HS}$ , is always much larger than  $L$ ; thus, the brushes are well-separated from each other. Meanwhile, the hard-sphere volume fraction  $\eta$ , i.e., the volume fraction of the correlated brushes, increases from 0.08 at 25 °C to 0.15 at 42 °C, implying a small enhancement of the correlation between the brushes upon heating. Above 42 °C, it steadily decreases to 0.1, which is attributed to the precipitation of the solution. In general, the low  $\eta$  values confirm the weak interaction between the brushes, which is consistent with their large distance.

The scattering features from the hard-sphere structure factor and the form factor, especially the cylinder length, cover a similar  $q$ -range (0.06–0.6 nm<sup>-1</sup>) because of the similar values of  $R_{HS}$  and  $L$ . However, the uncertainties of both values are low (Fig. 5a, c), and we are thus convinced that they can be determined reliably.

Scattering from large-scale inhomogeneities or aggregates is observed in the entire temperature range. Although the limited  $q$  range does not allow for characterization of their size, the Porod exponent  $\alpha$  can be evaluated and gives information regarding the compactness of the aggregates. From 25 to 36 °C,  $\alpha$  decreases slightly from 2.7 to 2.5, and increases abruptly to 3.1 at 38 °C (Fig. 6a). It stays at a value of ca. 3.0 and increases above  $T_{cp}$ , reaching 3.5 at 50 °C. Thus, below  $T_{cp}$ , the aggregates are mass fractals, i.e., they contain voids, while above  $T_{cp}$ , they transform into compact aggregates with rough surfaces. Our results are in line with previous studies on other molecular brush systems, which report that

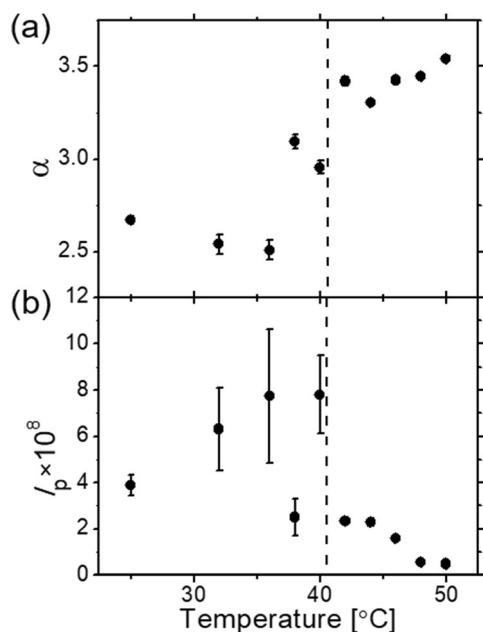


**Fig. 6** Parameters from the modified Porod term in the SANS data of the 30 g L<sup>-1</sup> solution of PiPOx<sub>100</sub>-g-PEtOx<sub>17</sub> in D<sub>2</sub>O in dependence on temperature. (a) Porod exponent  $\alpha$ . (b) Scaling factor  $I_p$ . The vertical dashed line indicates  $T_{cp}$  of the solution

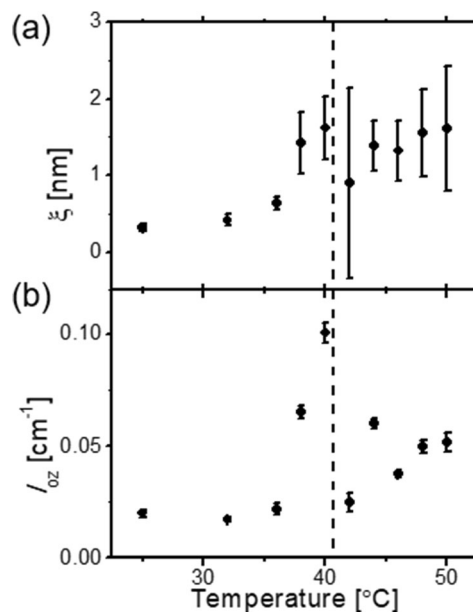


**Fig. 7** Parameters from the Ornstein-Zernike structure factor in the SANS data of the 30 g L<sup>-1</sup> solution of PiPOx<sub>100</sub>-g-PEtOx<sub>17</sub> in D<sub>2</sub>O in dependence on temperature. (a) Correlation length  $\xi$ . (b) Scaling factor  $I_{oz}$ . The vertical dashed line indicates  $T_{cp}$  of the solution

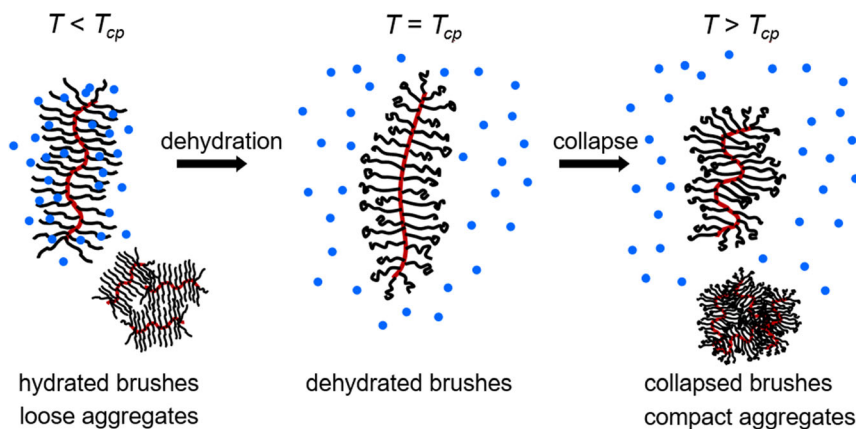


**Fig. 8** Schematic representation of the structural evolution of  $PiPOx_{100}\text{-}g\text{-}PEtOx_{17}$  in aqueous solution. The arrows indicate the heating process. The blue dots represent the water molecules

aggregates are present; both below and above the cloud point of the solution [10, 50–52]. We note that, in our system, not only the temperature-dependent properties of the PEtOx side chains play a role but also the hydrophobic NBocPip end groups may promote aggregation. The scaling factor of the modified Porod term  $I_p$  increases as the temperature approaches 40 °C (Fig. 6b), except for the value at 38 °C; however, the uncertainties are large. Considering the fact that, between 25 and 36 °C, there is no additional contribution from the individually dissolved brushes to the aggregates (Fig. 5b), the increase of  $I_p$  is possibly due to some rearrangement of the aggregates into larger ones with looser structure, thus leading to a slight decrease in their compactness (Fig. 6a). Above the cloud point, a drop of  $I_p$  is found, which is presumably due to the precipitation.

The Ornstein-Zernike structure factor describes the scattering from concentration fluctuations in the molecular brushes, most likely from the side chains. The correlation length  $\xi$  of these concentration fluctuations is 0.3 nm at 25 °C and increases to 1.6 nm at 40 °C, however, with large uncertainties (Fig. 7a). The increasing  $\xi$  indicates the dehydration of the side chains as the temperature is increased [39]. Correspondingly, the scaling factor of the Ornstein-Zernike term,  $I_{oz}$ , increases sharply, as the temperature approaches the cloud point (Fig. 7b), which is consistent with the increase of  $\xi$ . Above  $T_{cp}$ , the values are scattered, since the cylinder form factor overlaps with the Ornstein-Zernike contribution.

The proposed temperature-dependent structural changes of the brushes and the aggregates are schematically shown in Fig. 8. From room temperature to  $T_{cp}$ , the brushes stretch out due to dehydration of the side chains, which is reflected in the increased correlation length of the concentration fluctuations at small length scales. Above  $T_{cp}$ , the brushes collapse and shrink. Large aggregates, having sizes in the micrometer length scale, are present in the entire temperature range (from

25 to 50 °C, with  $T_{cp} = 40.5$  °C). Below  $T_{cp}$ , the aggregates are loosely structured, while above  $T_{cp}$ , they are compact.

## Conclusion

As evidenced by the experimental results from turbidimetry, DLS and SANS, the  $T_{cp}$  of the molecular brush with PEtOx side chains is 40.5 °C, thus significantly reduced compared with that of the oligomer PEtOx side chains ( $T_{cp} > 100$  °C). The huge suppression is attributed to both the dense grafting of the side chains to the backbone (virtually one side chain on every PiPOx backbone monomer) and the hydrophobic end groups on the side chains.

In the present study on a molecular brush with a specific ratio between the backbone length and the side chain length, a stretching of the molecular brush is discovered between room temperature and  $T_{cp}$ , before the brushes collapse upon further heating above  $T_{cp}$ . This two-step conformational change is attributed to the special molecular architecture, which is located between a star-like polymer and a bottlebrush polymer.

**Acknowledgments** This work is based upon experiments performed at the KWS-1 instrument operated by JCNS at the Heinz Maier-Leibnitz Zentrum (MLZ), Garching, Germany. MLZ is acknowledged for beam time allocation and for providing excellent equipment.

**Availability of data and material** N/A

**Code availability** N/A

**Authors' contributions** N/A

**Funding information** Open Access funding provided by Projekt DEAL. The authors received funding from Deutsche Forschungsgemeinschaft (PA 771/27-1). K. S. received financial support from the Erasmus Mundus master program MaMaSelf (Master in Materials Science Exploring Large Scale Facilities).

## Compliance with ethical standards

**Conflict of interest** The authors declare that they have no conflict of interest.

**Open Access** This article is licensed under a Creative Commons Attribution 4.0 International License, which permits use, sharing, adaptation, distribution and reproduction in any medium or format, as long as you give appropriate credit to the original author(s) and the source, provide a link to the Creative Commons licence, and indicate if changes were made. The images or other third party material in this article are included in the article's Creative Commons licence, unless indicated otherwise in a credit line to the material. If material is not included in the article's Creative Commons licence and your intended use is not permitted by statutory regulation or exceeds the permitted use, you will need to obtain permission directly from the copyright holder. To view a copy of this licence, visit <http://creativecommons.org/licenses/by/4.0/>.

## References

- Yuan J, Müller AHE, Matyjaszewski K, Sheiko SS (2012) 6.06 - molecular brushes. In: Matyjaszewski K, Möller M (eds) *Polymer science: a comprehensive reference*. Elsevier, Amsterdam
- Verduzco R, Li X, Pesek SL, Stein GE (2015) Structure, function, self-assembly, and applications of bottlebrush copolymers. *Chem Soc Rev* 44(8):2405–2420
- Johnson JA, Lu YY, Burts AO, Xia Y, Durrell AC, Tirrell DA, Grubbs RH (2010) Drug-loaded, bivalent-bottle-brush polymers by graft-through ROMP. *Macromolecules* 43(24):10326–10335
- Miki K, Kimura A, Oride K, Kuramochi Y, Matsuoka H, Harada H, Hiraoka M, Ohe K (2011) High-contrast fluorescence imaging of tumors in vivo using nanoparticles of amphiphilic brush-like copolymers produced by ROMP. *Angew Chem Int Ed* 50(29):6567–6570
- Miyake GM, Weitekamp RA, Piunova VA, Grubbs RH (2012) Synthesis of isocyanate-based brush block copolymers and their rapid self-assembly to infrared-reflecting photonic crystals. *J Am Chem Soc* 134(34):14249–14254
- Liberman-Martin AL, Chu CK, Grubbs RH (2017) Application of bottlebrush block copolymers as photonic crystals. *Macromol Rapid Commun* 38(13):1700058
- Abbasi M, Faust L, Wilhelm M (2019) Comb and bottlebrush polymers with superior rheological and mechanical properties. *Adv Mater* 31(26):1806484
- Cheng G, Melnichenko YB, Wignall GD, Hua F, Hong K, Mays JW (2008) Small angle neutron scattering study of conformation of oligo(ethylene glycol)-grafted polystyrene in dilute solutions: effect of the backbone length. *Macromolecules* 41(24):9831–9836
- Gromadzki D, Filippov S, Netopilik M, Makuška R, Jigounov A, Pleštil J, Horský J, Štěpánek P (2009) Combination of “living” nitroxide-mediated and photoiniferter-induced “grafting from” free-radical polymerizations: from branched copolymers to unimolecular micelles and microgels. *Eur Polym J* 45(6):1748–1758
- Weber C, Rogers S, Vollrath A, Hoepfner S, Rudolph T, Fritz N, Hoogenboom R, Schubert US (2013) Aqueous solution behavior of comb-shaped poly(2-ethyl-2-oxazoline). *J Polym Sci A Polym Chem* 51(1):139–148
- Pesek SL, Li X, Hammouda B, Hong K, Verduzco R (2013) Small-angle neutron scattering analysis of bottlebrush polymers prepared via grafting-through polymerization. *Macromolecules* 46(17):6998–7005
- Wu C, Wang X (1998) Globule-to-coil transition of a single homopolymer chain in solution. *Phys Rev Lett* 80(18):4092–4094
- Tavagnacco L, Zaccarelli E, Chiessi E (2018) On the molecular origin of the cooperative coil-to-globule transition of poly(*N*-isopropylacrylamide) in water. *Phys Chem Chem Phys* 20(15):9997–10010
- Bejagam KK, Singh SK, Ahn R, Deshmukh SA (2019) Unraveling the conformations of backbone and side chains in thermosensitive bottlebrush polymers. *Macromolecules* 52(23):9398–9408
- Li X, ShamsiJazeyi H, Pesek SL, Agrawal A, Hammouda B, Verduzco R (2014) Thermoresponsive PNIPAAm bottlebrush polymers with tailored side-chain length and end-group structure. *Soft Matter* 10(12):2008–2015
- Li C, Gunari N, Fischer K, Janshoff A, Schmidt M (2004) New perspectives for the design of molecular actuators: thermally induced collapse of single macromolecules from cylindrical brushes to spheres. *Angew Chem Int Ed* 43(9):1101–1104
- Hoogenboom R (2009) Poly(2-oxazolines): a polymer class with numerous potential applications. *Angew Chem Int Ed* 48(43):7978–7994
- Luxenhofer R, Han Y, Schulz A, Tong J, He Z, Kabanov AV, Jordan R (2012) Poly(2-oxazoline)s as polymer therapeutics. *Macromol Rapid Commun* 33(19):1613–1631
- Lorson T, Lübtow MM, Wegener E, Haider MS, Borova S, Nahm D, Jordan R, Sokolski-Papkov M, Kabanov AV, Luxenhofer R (2018) Poly(2-oxazolines) based biomaterials: a comprehensive and critical update. *Biomaterials* 178:204–280
- Lin P, Clash C, Pearce EM, Kwei TK, Aponte MA (1988) Solubility and miscibility of poly(ethyl oxazoline). *J Polym Sci B Polym Phys* 26(3):603–619
- Chen FP, Ames AE, Taylor LD (1990) Aqueous solutions of poly(ethyl-oxazoline) and its lower consolute phase transition. *Macromolecules* 23(21):4688–4695
- Christova D, Velichkova R, Loos W, Goethals EJ, Prez FD (2003) New thermo-responsive polymer materials based on poly(2-ethyl-2-oxazoline) segments. *Polymer* 44(8):2255–2261
- Hoogenboom R, Thijs HML, Jochems MJHC, van Lankvelt BM, Fijten MWM, Schubert US (2008) Tuning the LCST of poly(2-oxazolines) by varying composition and molecular weight: alternatives to poly(*N*-isopropylacrylamide)? *Chem Commun* 44:5758–5760
- Weber C, Becer CR, Hoogenboom R, Schubert US (2009) Lower critical solution temperature behavior of comb and graft shaped poly[oligo(2-ethyl-2-oxazoline)methacrylate]s. *Macromolecules* 42(8):2965–2971
- Kowalczyk A, Kronek J, Bosowska K, Trzebicka B, Dworak A (2011) Star poly(2-ethyl-2-oxazolines)—synthesis and thermosensitivity. *Polym Int* 60(7):1001–1009
- Filippov A, Tarabukina E, Kudryavtseva A, Fatullaev E, Kurlykin M, Tenkovtsev A (2019) Molecular brushes with poly-2-ethyl-2-oxazoline side chains and aromatic polyester backbone manifesting double stimuli responsiveness. *Colloid Polym Sci* 297(11):1445–1454
- Zhang N, Huber S, Schulz A, Luxenhofer R, Jordan R (2009) Cylindrical molecular brushes of poly(2-oxazolines) from 2-isopropenyl-2-oxazoline. *Macromolecules* 42(6):2215–2221
- Streitwieser A, Heathcock CH, Kosower EM, Corfield PJ (1992) *Introduction to organic chemistry*, vol 547 STR. Macmillan New York
- Štěpánek P (1993) Data analysis in dynamic light scattering. In: Brown W (ed) *Dynamic light scattering: the method and some applications (monographs on the physics and chemistry of materials)*. Clarendon Press, New York
- Jakeš J (1995) Regularized positive exponential sum (REPES) program - a way of inverting Laplace transform data obtained by dynamic light scattering. *Collect Czechoslov Chem Commun* 60:1781–1797
- Heinz Maier-Leibnitz Zentrum et al (2015) KWS-1: small-angle scattering diffractometer. *J Large-Scale Res Facil* 1:A28
- Feoktystov AV, Frielinghaus H, Di Z, Jaksch S, Pipich V, Appavou M-S, Babcock E, Hanslik R, Engels R, Kemmerling G, Kleines H, Ioffe A, Richter D, Brückel T (2015) KWS-1 high-resolution small-

- angle neutron scattering instrument at JCNS: current state. *J Appl Crystallogr* 48(1):61–70
33. Porod G (1951) Die Röntgenkleinwinkelstreuung von dichtgepackten kolloiden Systemen. *Kolloid-Zeitschrift* 124(2):83–114
  34. Roe R-J (2000) Small-angle scattering in: methods of X-ray and neutron scattering in polymer science. Oxford University Press, New York Oxford
  35. Onsager L (1949) The effects of shape on the interaction of colloidal particles. *Ann N Y Acad Sci* 51(4):627–659
  36. Fournet G (1951) Étude théorique et expérimentale de la diffusion des rayons X par les ensembles denses de particules. *Bull Soc Fr Mineral Cristallogr* 74:37–172
  37. Pedersen JS (1997) Analysis of small-angle scattering data from colloids and polymer solutions: modeling and least-squares fitting. *Adv Colloid Interf Sci* 70:171–210
  38. Percus JK, Yevick GJ (1958) Analysis of classical statistical mechanics by means of collective coordinates. *Phys Rev* 110(1):1–13
  39. Hammouda B, Ho DL (2007) Insight into chain dimensions in PEO/water solutions. *J Polym Sci B Polym Phys* 45(16):2196–2200
  40. Mass density of 2-Isopropenyl-2-oxazoline. <https://www.sigmaaldrich.com/catalog/product/aldrich/560626?lang=de&region=DE>. Accessed 25 May 2020
  41. Mass density of 2-Ethyl-2-oxazoline. <https://www.sigmaaldrich.com/catalog/product/aldrich/137456?lang=de&region=DE>. Accessed 25 May 2020
  42. Mass density of N-Boc-piperazine. <https://www.chemsrc.com/en/CasPaper/175702.html>. Accessed 25 May 2020
  43. <http://www.sasview.org/>. Accessed 01 March 2020
  44. Jerca FA, Jerca VV, Anghelache AM, Vuluga DM, Hoogenboom R (2018) Poly(2-isopropenyl-2-oxazoline) as a versatile platform towards thermoresponsive copolymers. *Polym Chem* 9(25):3473–3478
  45. Zhou Y, Tang H, Wu P (2017) Intra-molecular interactions dominating the dehydration of a poly(2-isopropyl-2-oxazoline)-based densely grafted polymer comb in aqueous solution and hysteretic liquid–liquid phase separation. *Phys Chem Chem Phys* 19(9):6626–6635
  46. logP value for the tert-butyloxycarbonyl end group. <https://www.chemspider.com/Chemical-Structure.126561.html>. Accessed 5 Jun 2020
  47. logP value for the tert-butyloxycarbonyl end group. [http://www.molbase.com/en/synthesis\\_57260-71-6-moldata-1516172.html](http://www.molbase.com/en/synthesis_57260-71-6-moldata-1516172.html). Accessed 5 Jun 2020
  48. Pesek SL, Xiang Q, Hammouda B, Verduzco R (2017) Small-angle neutron scattering analysis of bottlebrush backbone and side chain flexibility. *J Polym Sci B Polym Phys* 55(1):104–111
  49. Yim H, Kent MS, Satija S, Mendez S, Balamurugan SS, Balamurugan S, Lopez GP (2005) Evidence for vertical phase separation in densely grafted, high-molecular-weight poly(*N*-isopropylacrylamide) brushes in water. *Phys Rev E* 72(5):051801
  50. Cheng G, Melnichenko YB, Wignall GD, Hua F, Hong K, Mays JW (2007) Conformation of oligo(ethylene glycol) grafted polystyrene in dilute aqueous solutions. *Polymer* 48(14):4108–4113
  51. Hussain H, Mya KY, He C (2008) Self-assembly of brush-like poly[poly(ethylene glycol) methyl ether methacrylate] synthesized via aqueous atom transfer radical polymerization. *Langmuir* 24(23):13279–13286
  52. Zhao J, Zhang G, Pispas S (2010) Thermoresponsive brush copolymers with poly(propylene oxide-*ran*-ethylene oxide) side chains via metal-free anionic polymerization “grafting from” technique. *J Polym Sci, Part A: Polym Chem* 48(11):2320–2328

**Publisher's note** Springer Nature remains neutral with regard to jurisdictional claims in published maps and institutional affiliations.